3D PRINTING

Scalable submicrometer additive manufacturing

Sourabh K. Saha[1]*†‡, Dien Wang[2]*, Vu H. Nguyen[1]*, Yina Chang[2], James S. Oakdale[1], Shih-Chi Chen[2]‡

High-throughput fabrication techniques for generating arbitrarily complex three-dimensional structures with nanoscale features are desirable across a broad range of applications. Two-photon lithography (TPL)–based submicrometer additive manufacturing is a promising candidate to fill this gap. However, the serial point-by-point writing scheme of TPL is too slow for many applications. Attempts at parallelization either do not have submicrometer resolution or cannot pattern complex structures. We overcome these difficulties by spatially and temporally focusing an ultrafast laser to implement a projection-based layer-by-layer parallelization. This increases the throughput up to three orders of magnitude and expands the geometric design space. We demonstrate this by printing, within single-digit millisecond time scales, nanowires with widths smaller than 175 nanometers over an area one million times larger than the cross-sectional area.

Nanoscale device development requires scaling up nanofabrication of arbitrarily complex three-dimensional (3D) structures. The photopolymerization-based, submicrometer additive manufacturing two-photon lithography (TPL) technique generates 3D structures with features on the scale of 200 nm (*1*). The production rate is faster than high-resolution 2D techniques such as e-beam lithography (*2*, *3*). TPL relies on nonlinear two-photon absorption to generate features smaller than the diffraction-limited focused light spot (*4*–*6*). This capability allows fabrication of functional micro- and nanoscale 3D structures, such as photonic crystals (*7*, *8*), mechanical metamaterials (*9*–*12*), micromachines (*13*, *14*), miniaturized optics (*15*), flexible electronics (*16*), and bioscaffolds (*17*). Serially scanning a tightly focused laser spot in a photopolymer resist to fabricate 3D structures by overlapping the individual submicrometer volumetric pixels (i.e., voxels) is the most common implementation. This serial and slow writing scheme makes large-scale production impractical. As a result, the adoption of TPL is mostly limited to academic and research laboratories. We show that a rate increase of two to three orders of magnitude is possible without compromising the submicrometer resolution by parallel TPL processing based on femtosecond projection. Our method allows access to difficult-to-explore regions in design space, increasing both the potential for cost-effective high-throughput processing and the geometric complexity of the printed objects.

Parallelizing TPL while maintaining the capability to print arbitrarily complex 3D patterns is challenging because of the specific nature of femtosecond light-matter interactions. Femtosecond pulsed lasers are necessary for TPL because appreciable two-photon absorption in photopolymers requires light intensity on the order of ~1 TW/cm^2 (*5*, *18*). Focusing an ultrafast pulsed laser beam into a small spot achieves this high intensity. Parallel printing requires strategies like structuring the light beam to project an arbitrary 2D pattern or generating multiple focal spots to multiply the writing speed during point scanning. However, improving the fabrication throughput without compromising the resolution and/or the pattern complexity is challenging. For example, some past attempts at parallelizing TPL via projection of images from tunable digital masks have failed to achieve the submicrometer depth resolution that is routinely achievable in serial writing (*19*). Holographic methods developed to generate and scan multiple focal spots simultaneously (*20*, *21*) cannot fabricate arbitrary structures, so they are mostly suitable for printing periodic structures. We developed a femtosecond projection TPL (FP-TPL) technique that ensures simultaneous spatial and temporal focusing of ultrafast light to achieve parallel printing of arbitrarily complex 3D structures with submicrometer resolution.

We fabricated 3D structures using a layer-by-layer printing of patterned 2D layers ranging in thickness from less than 1 μm to more than 4 μm. Each 2D layer was up to 165 μm × 165 μm in size and was written in millisecond

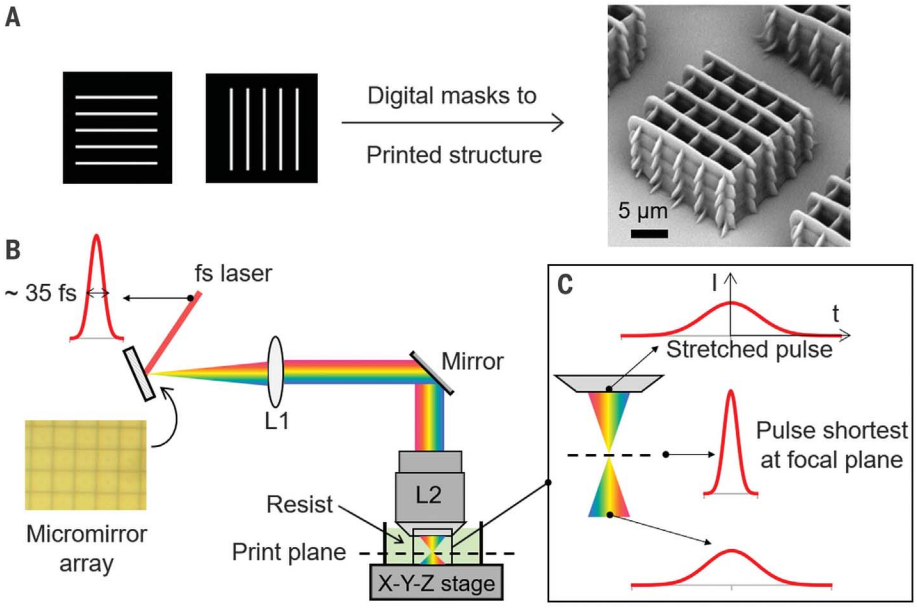

Fig. 1. Femtosecond projection TPL based on spatial and temporal focusing. (**A**) 3D printing with submicrometer resolution using layer-by-layer projection of digital masks. (**B**) Schematic of the fabrication setup. 2D layers are printed by projecting an image of the micromirror array onto the print plane within the photopolymer resist. Printing can be restricted to layers of <1 μm thickness by generating strong intensity gradients through temporal focusing of the femtosecond (fs) laser. L1 refers to the collimating lens and L2 refers to the objective lens. Femtosecond pulses are stretched and compressed as they pass through the optical system to implement temporal focusing. The micromirror array spectrally separates the different wavelengths of the femtosecond pulse and stretches it, whereas the objective lens focuses the pulse in the time domain. The micromirror array, L1, and L2 are set up in a 4*f*-like optical arrangement to ensure that the optical path lengths for all wavelengths are equal between the micromirror array and the focal plane of the objective lens L2 but unequal across different wavelengths between other points. (**C**) Zoomed-in schematic of temporal focusing in the focal volume of the objective lens, where the shortest pulse is only achieved at the focal (build) plane. *I*, intensity; *t*, time.

[1]Center for Engineered Materials and Manufacturing, Lawrence Livermore National Laboratory, Livermore, CA, USA.
[2]Department of Mechanical and Automation Engineering, The Chinese University of Hong Kong, Shatin, Hong Kong.
*These authors contributed equally to this work.
†Present address: Woodruff School of Mechanical Engineering, Georgia Institute of Technology, Atlanta, GA 30332, USA.
‡Corresponding author. Email: sourabh.saha@me.gatech.edu (S.K.S.); scchen@mae.cuhk.edu.hk (S.-C.C.)

time scales. We generated such thin 2D layers by projecting a patterned 2D light sheet (equivalent to a planar point cloud containing more than a million points) that was focused in both the space and time domains. We can pattern the light sheet into arbitrary 2D patterns through a digital micromirror device (DMD), a standard grating-like component of digital light projectors. We harnessed the broadband nature of femtosecond lasers and diffraction from the DMD to achieve focusing in the time domain. During temporal focusing, a prestretched ultrashort light pulse is progressively shortened as it travels through the photopolymer resist so that the shortest pulse (the highest light intensity) is achieved only at the spatial focal plane. The intensity gradient generated through temporal focusing ensures that writing is spatially restricted to the focal plane, without causing polymerization above or below the focal plane (Fig. 1). Without this temporal focusing, depth resolution is lost. Instead of forming a thin sheet, all the material in the path of the projected beam polymerizes to form thick extruded solid structures similar to those formed in previous parallelization demonstrations (*19*). We consistently and reliably printed subdiffraction 3D structures over large areas by exploiting the ultrathin and uniform femtosecond light sheet and the optimized voxel aspect ratio.

We generated near-infrared femtosecond pulses with a broad wavelength spectrum (approximately tens of nanometers) with our laser source that provided the light to drive the writing process. We patterned the light beam by illuminating the digital mask, which was an array of individually switchable micromirrors. The intensity of light emerging from a micromirror along a predetermined direction was high when switched on and low when switched off. We then collimated the diverging beam that emerges from the DMD. The collimated beam passes through the objective lens and was focused onto a plane inside the photopolymer resist material. When projected onto the image plane, the switched-on points from the DMD had light intensities above the polymerization threshold, writing a pixelated image of the digital mask in the resist. This image contained distinct or overlapping cured voxels. We fabricated 3D structures by moving the focused image plane relative to the resist with motion stages (Fig. 2).

Although our FP-TPL technique appears similar in approach to that of single-photon projection stereolithography techniques (*22*), we implemented a fundamentally different projection mechanism. This difference accounts for the spatially coherent broadband laser source used in the FP-TPL system. As the DMD-based digital mask is a dispersive element owing to its periodic micromirror array structure, spatially coherent light diffracts upon hitting the DMD to generate several distinct emergent beams. Because of the broadband nature of femtosecond laser light, the diffracted beams for the different wavelengths emerge at slightly different angles. This spectral separation of light is accompanied by a stretching of the pulse duration, which is a widely exploited phenomenon in the design of high-power ultrafast lasers (*23*). Unless properly compensated, this pulse stretching may lead to a loss in the intensity gradient at the focal plane of the objective lens. The temporal focusing technique ensures that the pulse is compressed back to the shortest duration only at the spatial focal plane of the objective lens. This generates a strong intensity gradient at the spatial focal plane that restricts polymerization within a thin layer centered at the focal plane.

We have achieved temporal focusing through an optical arrangement wherein the focused image plane of the objective lens is the conjugate plane of the digital mask. This ensures that the optical path lengths for the different wavelengths of the femtosecond laser emerging from the mask are identical at the focal plane but unequal everywhere else. The full spectrum of the laser therefore spatially overlaps only at the focal plane, thereby leading to the shortest pulse at the focal plane. Temporal focusing has been used for imaging and manufacturing applications where nontunable diffraction gratings spectrally separate light (*24*–*27*). These fixed-mask techniques cannot be used for additive manufacturing. We use the DMD-based digital mask as both the light structuring device and as the diffraction grating. We previously demonstrated that this

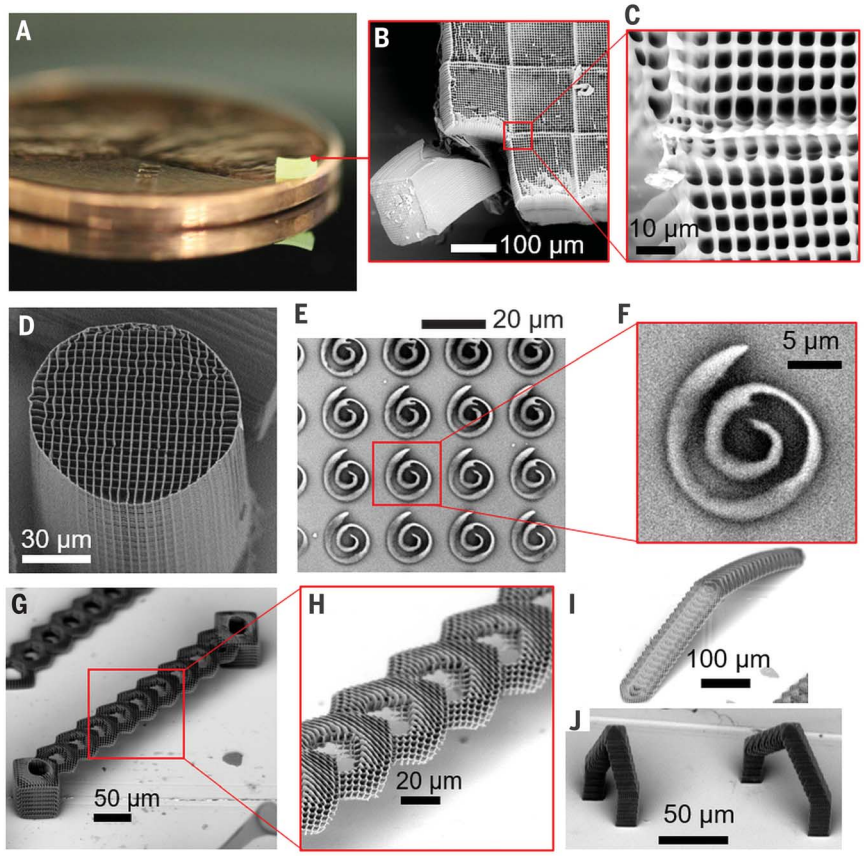

Fig. 2. Printing of complex 3D structures with submicrometer resolution via femtosecond projection TPL. (**A** to **C**) Millimeter-scale structure with submicrometer features supported on a U.S. penny on top of a reflective surface. The 2.20 mm × 2.20 mm × 0.25 mm cuboid was printed in 8 min 20 s, demonstrating a 3D printing rate of 8.7 mm^3/hour. In contrast, serial techniques would require several hours to print this cuboid. (**D**) A 3D micropillar printed through stacking of 2D layers, demonstrating uniformity of printing that is indistinguishable from that of commercial serial-scanning systems. (**E** and **F**) Spiral structures printed through projection of a single layer demonstrating the ability to rapidly print curvilinear structures within single-digit millisecond time scales without any stage motion. (**G** to **J**) Overhanging 3D structures printed by stitching multiple 2D projections demonstrating the ability to print depth-resolved features. The bridge structure in (G), with 90° overhang angles, is challenging to print using serial-scanning TPL techniques or any other technique owing to its large overhang relative to the size of the smallest feature and the submicrometer feature resolution.

temporal focusing scheme can be used for material removal processes (*28*, *29*).

We have quantified the resolution limit of FP-TPL by developing a computational model of light propagation that predicts the light intensity distribution in the focal volume. We obtained the temporally focused intensity distribution by simulating the propagation of a broadband femtosecond pulse through the optical system (*30*). We found that temporal focusing allows for submicrometer full width at half maximum (FWHM) axial thickness (figs. S4 and S5). The aspect ratio of the voxels we induced by projecting DMD pixels was closer to 1 and smaller than the typical point spread function of serial scanning systems. This provides substantial advantage in terms of resolution and structural strength when fabricating subdiffraction structures. We projected each DMD pixel to an area of 151 nm × 151 nm in the work field and generated light spots of various sizes by tuning the pattern on the DMD (fig. S4). The nonlinear photoabsorption mechanism and the resist's thresholding behavior ensures that features smaller than the optical diffraction limit can be fabricated with light spots of various sizes.

We printed nanowire features thinner than the optical diffraction limit along both the lateral and the axial dimensions by varying the projected line thickness, the beam power, and the duration of exposure. We printed nanowires with lateral widths as thin as 130 to 140 nm and with an axial height as short as 175 nm (Fig. 3). These features are thinner than other parallel multiphoton printed polymer nanowires (*19*, *31*, *32*) and comparable in width to serial scanning TPL systems (*1*). The 175 nm height of the thinnest line is smaller than past demonstrations of both parallel and serial TPL (*1*). Our result of a 1.25 voxel aspect ratio confirmed our model prediction of an aspect ratio of ~1. We observed that the feature size increases with the dosage D, where $D \sim t_{exp}^{m} \times I^{n}$ in TPL. The exposure (t_{exp}) and the intensity (I) are scaled with parameters $m \leq 1$ and $n \geq 2$. The feature size increases with the dosage above a threshold dosage for polymerization. Features smaller than the optical FWHM width can be generated under low dosage conditions (Fig. 3). This feature size versus dosage dependence is similar to that observed in the serial single-spot TPL process (*33*).

A peculiarity of our projection scheme is that the size of a contiguous projected feature can be controlled over a wide range. This change in the projected feature size alters the scaling of the lithographically generated feature size versus the optical FWHM (Fig. 3). For very thin features (3 pixels wide), the line width stays below the optical FWHM width for a wider range of exposure time. In contrast, line

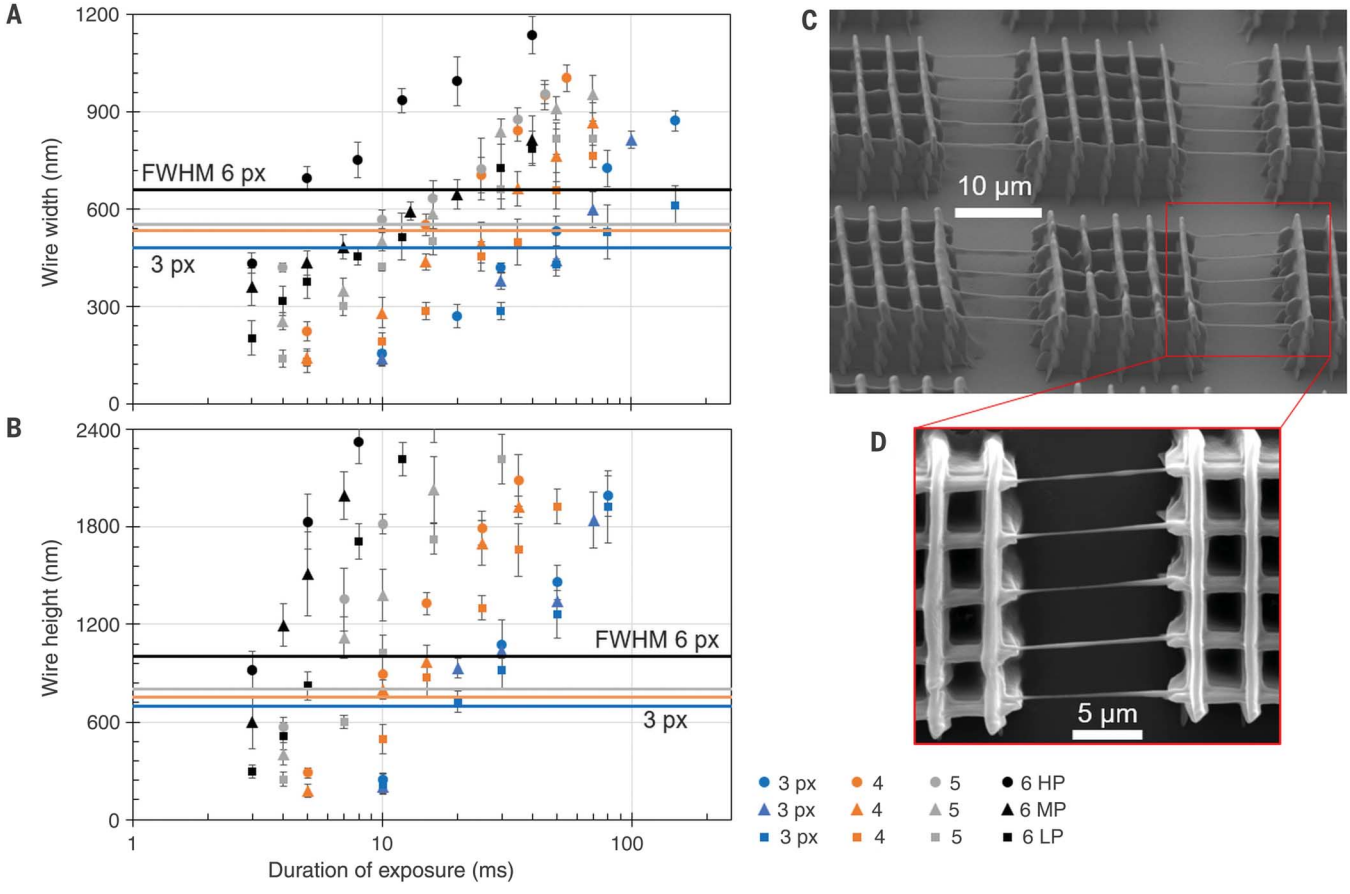

Fig. 3. Printed nanowires demonstrating nanoscale resolution of FP-TPL. (**A**) Width (along lateral direction) and (**B**) height (along axial direction) of suspended nanowires printed under different conditions. Width of lines in the projected DMD pattern was varied from 3 to 6 pixels with a fixed period of 30 pixels. Each pixel (px) maps to 151 nm in the projected image. Labels HP, MP, and LP refer to high (42 nW/px), medium (39 nW/px), and low (35 nW/px) power levels, respectively, wherein time-averaged power was measured immediately before the aperture of the objective lens. All markers of a specific shape represent data points generated at the same power level, and all markers of a specific color represent the same line width. Horizontal lines are the FWHM width and height of the light intensity distributions obtained from simulations of fig. S4. Printing was performed with a femtosecond laser that had a center wavelength of 800 nm and a nominal pulse width of 35 fs and with a 60× 1.25 numerical aperture objective lens. Error bars quantify the 1 SD in a sample size of five wires printed simultaneously in the same projection. (**C** and **D**) Scanning electron microscope images of the suspended nanowire features.

width exceeds the optical FWHM width for thicker features (6-pixel, high-power condition) even under low exposure conditions. We believe that this size-dependent behavior originates from the radical-mediated photopolymerization mechanism underlying this process. Our hypothesis is supported by the observation that the writing threshold exposure is lower for thicker projected features (fig. S10). Photoactivated radicals generated in the smaller exposed regions of the photoresist can be rapidly quenched by the oxygen and radical inhibitor species diffusing in from the surrounding unexposed regions. However, quenching of radicals is less likely in the central region of a large illuminated area owing to depletion of the quenchers over the entire area. A similar size-dependent thresholding behavior, which we call the self-proximity effect, has also been observed in volumetric photopolymerization processes wherein a large volume is simultaneously exposed at once (*34*).

The self-proximity effect also explains the thicker wire heights than the axial optical FWHM width even for writing conditions when the wire widths are smaller than the lateral optical FWHM width. A nonzero background intensity exists along the axial direction owing to the projection mechanism, whereas a zero background intensity level exists in the nonprojected sections on the $z = 0$ plane (fig. S4B). This nonzero background intensity along the axial direction causes the wire heights to be larger than the wire widths when normalized by the respective optical FWHM widths. The nonzero background intensity is undesirable for printing of thin features but may be used to print complex features through dosage accumulation as is used in the computed axial lithography volumetric additive manufacturing technique (*35*). In the context of FP-TPL, the consequence of this self-proximity effect is that (i) if fast writing of thin features is desired, one must print under low-exposure conditions with moderately large projected feature sizes, and (ii) the exposure must be varied across a projection area to achieve uniform printing of structures comprising nonuniform feature sizes (fig. S11).

During scaling of the TPL process from the serial to the parallel format, the intensity at each focal volume is similar (approximately terawatts per square centimeter). However, the total energy incident on the photopolymer material does not scale by the number of focal spots. Instead, the actual incident beam energy in the parallel format is four orders of magnitude smaller than one would estimate by linearly scaling the energy of serial-scanning spot by the number of focal spots (table S3). This discrepancy is the result of the underlying chain reaction–type radical-mediated photopolymerization mechanism of TPL being sensitive to the light intensity for the initiation of reactions, but sustained photoenergy is not needed for the reactions to proceed (*36*). Using a 1-kHz repetition rate commercially available ultrafast laser with a high (~1 mJ) pulse energy takes advantage of this underlying photopolymerization mechanism to achieve massive parallelization by ensuring focal spot intensities of approximately terawatts per square centimeter.

The throughput of FP-TPL is insensitive to the number of voxels written per layer because of its ability to project an entire 2D layer at once. The area of projection, layer thickness, and the time interval between projection of subsequent layers determines the volumetric throughput of FP-TPL. The area of projection and the duration of exposure per projection determines the areal throughput. For our system, we can project up to ~1 million pixels per exposure, and the maximum area of projection is 165 μm × 165 μm. We can vary the layer thickness from <1 μm up to ~4 μm, and the time interval between projection of subsequent layers is 20 ms. This includes the time taken for stage motion. The duration of exposure per projection lies in the 3-ms range. The voxel generation rate is ~333 million voxels/s, areal 2D printing rate is ~9 mm^2/s, the single-layer FP-TPL has a volumetric processing rate between 33 and 131 mm^3/hour, and the volumetric 3D printing rate is between 5 and 20 mm^3/hour. The rates are for printing configurations that maintain the submicrometer in-plane (lateral) printing resolution and are independent of the in-plane geometry of the layers.

We compare our FP-TPL performance with previous TPL demonstrations (Fig. 4). The single-layer volumetric processing rate of FP-TPL exceeds that of the existing serial techniques by at least three orders of magnitude while maintaining sub-500-nm features. Our 3D printing rate exceeds that of the fastest serial system by more than 90 times for porous structures and by more than 450 times for nonporous structures (supplementary materials, supplementary text S15). The FP-TPL method is also capable of patterning arbitrarily complex 3D structures while maintaining the submicrometer feature sizes. In addition, the temporally focused light sheet in FP-TPL enables achieving high out-of-plane (axial) resolution. Another attractive feature of FP-TPL compared with the serial writing technique is the ability to project and print curvilinear features (Fig. 2E) without requiring stage accelerations and decelerations during the piecewise linear path discretization approximations. This substantially increases the throughput. The areal projection mechanism also enables printing of long suspended bridge structures with 90° overhangs (Fig. 2G). Overhanging structures are challenging to print using a serial-scanning technique because of feature drift during the long printing process. We expect that the throughput, resolution, and pattern flexibility of FP-TPL makes it

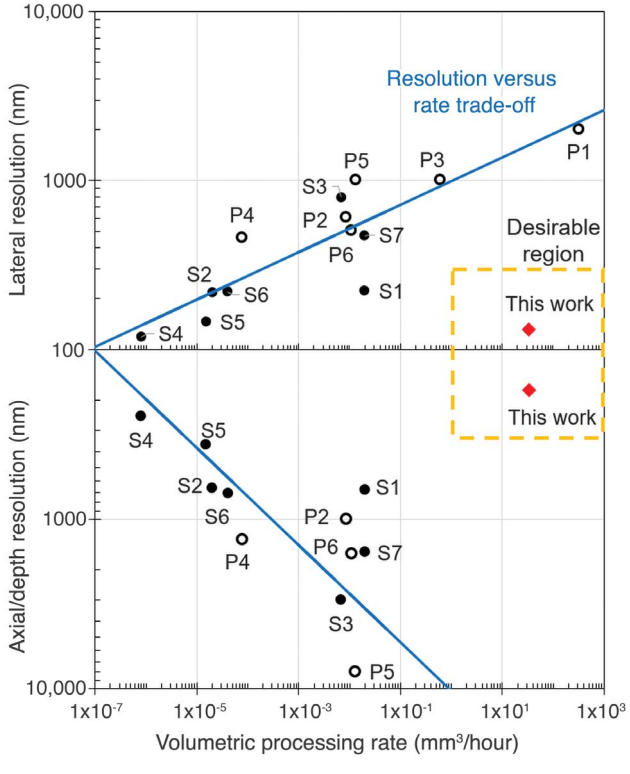

Fig. 4. Comparison of rate and resolution of FP-TPL with past demonstrations of TPL. S1 to S7 are instances of serial TPL implementation and P1 to P6 are instances of parallel TPL. P1 and P3 are not shown in the lower plot because they have an axial (depth) resolution higher than 10 μm. Protocol for evaluation of the volumetric processing rate is available in supplementary text S15. FP-TPL breaks the traditional resolution versus rate trade-offs. Literature references are as follows: S1, Oakdale *et al*. (*2*); S2, Meza *et al*. (*11*); S3, Shaw *et al*. (*37*); S4, Lu *et al*. (*1*); S5, Fischer *et al*. (*6*); S6, Malinauskas *et al*. (*5*); S7, Jonušauskas *et al*. (*38*); P1, Mills *et al*. (*19*); P2, Li *et al*. (*32*); P3, Yang *et al*. (*31*); P4, Vizsnyiczai *et al*. (*20*); P5, Yang *et al*. (*21*); and P6, Geng *et al*. (*39*).

an attractive technology to scale up the fabrication of functional micro- and nanostructures such as mechanical and optical metamaterials, micro-optics, bioscaffolds, electrochemical interfaces, and flexible electronics—technology that may play a large role in fields such as electric transportation, healthcare, clean energy and water, computing, and telecommunications.

REFERENCES AND NOTES

1. W.-E. Lu, X.-Z. Dong, W.-Q. Chen, Z.-S. Zhao, X.-M. Duan, *J. Mater. Chem.* **21**, 5650–5659 (2011).
2. J. S. Oakdale *et al.*, *Adv. Funct. Mater.* **27**, 1702425 (2017).
3. M. Altissimo, *Biomicrofluidics* **4**, 026503 (2010).
4. S. Maruo, O. Nakamura, S. Kawata, *Opt. Lett.* **22**, 132–134 (1997).
5. M. Malinauskas, A. Žukauskas, G. Bičkauskaitė, R. Gadonas, S. Juodkazis, *Opt. Express* **18**, 10209–10221 (2010).
6. J. Fischer *et al.*, *Opt. Express* **21**, 26244–26260 (2013).
7. S. Juodkazis, V. Mizeikis, K. K. Seet, H. Misawa, U. G. Wegst, *Appl. Phys. Lett.* **91**, 241904 (2007).
8. G. von Freymann *et al.*, *Adv. Funct. Mater.* **20**, 1038–1052 (2010).
9. J. Bauer *et al.*, *Adv. Mater.* **29**, 1701850 (2017).
10. T. Frenzel, M. Kadic, M. Wegener, *Science* **358**, 1072–1074 (2017).
11. L. R. Meza, S. Das, J. R. Greer, *Science* **345**, 1322–1326 (2014).
12. J. Bauer, A. Schroer, R. Schwaiger, O. Kraft, *Nat. Mater.* **15**, 438–443 (2016).
13. T.-Y. Huang *et al.*, *Adv. Mater.* **27**, 6644–6650 (2015).
14. S. Maruo, H. Inoue, *Appl. Phys. Lett.* **89**, 144101 (2006).
15. T. Gissibl, S. Thiele, A. Herkommer, H. Giessen, *Nat. Photonics* **10**, 554–560 (2016).
16. W. Xiong *et al.*, *Adv. Mater.* **28**, 2002–2009 (2016).
17. A. Selimis, V. Mironov, M. Farsari, *Microelectron. Eng.* **132**, 83–89 (2015).
18. H.-B. Sun, S. Kawata, *Adv. Polym. Sci.* **170**, 169–273 (2004).
19. B. Mills, J. A. Grant-Jacob, M. Feinaeugle, R. W. Eason, *Opt. Express* **21**, 14853–14858 (2013).
20. G. Vizsnyiczai, L. Kelemen, P. Ormos, *Opt. Express* **22**, 24217–24223 (2014).
21. L. Yang *et al.*, *Opt. Lasers Eng.* **70**, 26–32 (2015).
22. X. Zheng *et al.*, *Rev. Sci. Instrum.* **83**, 125001 (2012).
23. D. Strickland, G. Mourou, *Opt. Commun.* **55**, 447–449 (1985).
24. D. Oron, E. Tal, Y. Silberberg, *Opt. Express* **13**, 1468–1476 (2005).
25. G. Zhu, J. van Howe, M. Durst, W. Zipfel, C. Xu, *Opt. Express* **13**, 2153–2159 (2005).
26. D. Kim, P. T. So, *Opt. Lett.* **35**, 1602–1604 (2010).
27. J.-N. Yih *et al.*, *Opt. Lett.* **39**, 3134–3137 (2014).
28. C. Gu *et al.*, *Precis. Eng.* **50**, 198–203 (2017).
29. D. Wang, C. Wen, Y. Chang, W. Lin, S.-C. Chen, *Precis. Eng.* **52**, 106–111 (2018).
30. Materials and methods are available as supplementary materials.
31. L. Yang *et al.*, *Opt. Commun.* **331**, 82–86 (2014).
32. Y.-C. Li *et al.*, *Opt. Express* **20**, 19030–19038 (2012).
33. J. Serbin *et al.*, *Opt. Lett.* **28**, 301–303 (2003).
34. M. Shusteff *et al.*, *Sci. Adv.* **3**, o5496 (2017).
35. B. E. Kelly *et al.*, *Science* **363**, 1075–1079 (2019).
36. J. B. Mueller, J. Fischer, F. Mayer, M. Kadic, M. Wegener, *Adv. Mater.* **26**, 6566–6571 (2014).
37. L. A. Shaw *et al.*, *Opt. Express* **26**, 13543–13548 (2018).
38. L. Jonušauskas *et al.*, *Opt. Express* **27**, 15205–15221 (2019).
39. Q. Geng, D. Wang, P. Chen, S.-C. Chen, *Nat. Commun.* **10**, 2179 (2019).

ACKNOWLEDGMENTS

We thank R. Panas and C. Spadaccini at Lawrence Livermore National Laboratory (LLNL) for helpful discussions and B. Au at LLNL for technical support. **Funding:** This work was performed under the auspices of the U.S. Department of Energy by LLNL under contract DE-AC52-07NA27344 and by The Chinese University of Hong Kong (CUHK) under subcontracts. (Document release LLNL-JRNL-770497). Funding was provided by LLNL's LDRD project 16-ERD-047. The work at CUHK was partially supported by HKSAR Research Grants Council (RGC), General Research Fund (GRF) 14209081 and 14206517. **Author contributions:** S.K.S. and S.-C.C. conceived of and designed the study. D.W., V.H.N., and S.K.S. set up the FP-TPL systems and performed the FP-TPL experiments. V.H.N. designed and developed the electronic hardware and control system at LLNL. S.K.S. and Y.C. performed the optics simulations. J.S.O. synthesized the photopolymer resists and performed SEM imaging of nanowires. S.K.S., S.-C.C., and V.H.N. analyzed the results. S.K.S. prepared the manuscript with input from all coauthors, and all coauthors edited the manuscript. S.K.S. supervised the work at LLNL, and S.-C.C. supervised the work at CUHK. **Competing interests:** Patent applications related to this work have been filed at the U.S. Patent and Trademark Office with S.K.S. and S.-C.C. as co-inventors and assigned to Lawrence Livermore National Security, LLC. All authors declare that they have no other competing interests. **Data and materials availability:** All data are available in the manuscript or the supplementary materials.

SUPPLEMENTARY MATERIALS

science.sciencemag.org/content/366/6461/105/suppl/DC1
Materials and Methods
Supplementary Text
Figs. S1 to S16
Tables S1 to S6
References (*40*–*45*)
Movie S1

30 April 2019; accepted 9 September 2019
10.1126/science.aax8760

Scalable submicrometer additive manufacturing

Sourabh K. Saha, Dien Wang, Vu H. Nguyen, Yina Chang, James S. Oakdale, and Shih-Chi Chen

Science, **366** (6461), .
DOI: 10.1126/science.aax8760

Speeding up submicrometer printing

Using light to build three-dimensional structures with photopolymerization is the basis for two-photon lithography. However, there has been a trade-off between speed and resolution for fabricating structures with this method. Saha *et al.* optimize a new parallel printing methodology that relies on ultrafast lasers. They show the ability to dramatically increase the speed of printing while maintaining submicrometer resolution.

Science, this issue p. 105